

# We are IntechOpen, the world's leading publisher of Open Access books Built by scientists, for scientists

3,900

Open access books available

116,000

International authors and editors

120M

Downloads

Our authors are among the

154

Countries delivered to

TOP 1%

most cited scientists

12.2%

Contributors from top 500 universities



WEB OF SCIENCE™

Selection of our books indexed in the Book Citation Index  
in Web of Science™ Core Collection (BKCI)

Interested in publishing with us?  
Contact [book.department@intechopen.com](mailto:book.department@intechopen.com)

Numbers displayed above are based on latest data collected.  
For more information visit [www.intechopen.com](http://www.intechopen.com)



# First-Principles Study of $ABO_3$ : Role of the $B-O$ Coulomb Repulsions for Ferroelectricity and Piezoelectricity

Kaoru Miura

Corporate R&D Headquarters, Canon Inc., Shimomaruko, Ohta, Tokyo  
Japan

## 1. Introduction

Since Cohen (Cohen & Krakauer, 1990; Cohen, 1992) proposed an origin for ferroelectricity in perovskite oxides, investigations of ferroelectric materials using first-principles calculations have been extensively studied (Ahart et al., 2008; Bévilion et al., 2007; Bousquet et al., 2006; Chen et al., 2004; Diéguez et al., 2005; Furuta & Miura, 2010; Khenata et al., 2005; Kornev et al., 2005; Miura & Tanaka, 1998; Miura, 2002; Miura et al., 2009; 2010a;b; Miura & Furuta, 2010; Miura et al., 2011; Oguchi et al., 2009; Ricinski et al., 2006; Uratani et al., 2008; Vanderbilt, 2000; Z. Wu et al., 2005). Currently, using the pseudopotential (PP) methods, most of the crystal structures in ferroelectric perovskite oxides ( $ABO_3$ ) as well as perovskite-related oxides can be precisely predicted. However, it is also known that the most stable structures of  $ABO_3$  optimized by the first-principles PP methods are sometimes inconsistent with the experimental results.

$BaTiO_3$  is a well-known ferroelectric  $ABO_3$ , and shows the tetragonal structure at room temperature. However, even in this well-known material, the optimized structure by the PP methods of first-principles calculations is strongly dependent on the choice of the Ti PPs, i.e., preparation for Ti 3s and 3p semicore states in addition to Ti 3d and 4s valence states is essential to the appearance of the tetragonal structure. This is an important problem for ferroelectricity, but it has been generally recognized for a long time that this problem is within an empirical framework of the calculational technics (Gonze et al., 2005).

It is known that ferroelectric state appears when the long-range forces due to the dipole-dipole interaction overcome the short-range forces due to the Coulomb repulsions. Cohen (Cohen & Krakauer, 1990; Cohen, 1992) proposed that the hybridization between Ti 3d state and O 2p state (Ti 3d–O 2p) in  $BaTiO_3$  and  $PbTiO_3$ , which weakens the short-range force of the Coulomb repulsions between Ti and O ions, is origin of ferroelectricity. However, it seems to be difficult to consider explicitly whether the long-range force due to the dipole-dipole interaction can or cannot overcome the short-range force only with the Ti 3d–O 2p hybridization. Investigations about the relationship between the Ti–O Coulomb repulsions and the appearance of ferroelectricity were separately reported. Theoretically, we previously investigated (Miura & Tanaka, 1998) the influence of the Ti– $O_z$  Coulomb repulsions on Ti ion displacement in tetragonal  $BaTiO_3$  and  $PbTiO_3$ , where  $O_z$  denotes the O atom to the z-axis (Ti is displaced to the z-axis). Whereas the hybridization between Ti 3d state and  $O_z$  2p<sub>z</sub> state stabilize Ti ion displacement, the strong Coulomb repulsions between Ti 3s and 3p<sub>z</sub>

states and O  $2p_z$  states do not favourably cause Ti ion displacement. Experimentally, on the other hand, Kuroiwa *et al.* (Kuroiwa *et al.*, 2001) showed that the appearance of ferroelectric state is closely related to the total charge density of Ti–O bondings in  $\text{BaTiO}_3$ . As discussed above, investigation about a role of Ti 3s and 3p states is important in the appearance of the ferroelectric state in tetragonal  $\text{BaTiO}_3$ .

It has been generally known (Miura & Furuta, 2010) that the most stable structure of  $\text{ABO}_3$  is closely related to the tolerance factor  $t$ ,

$$t \equiv \frac{r_A + r_O}{\sqrt{2}(r_B + r_O)}, \quad (1)$$

where  $r_A$ ,  $r_B$ , and  $r_O$  denote the ionic radii of A, B, and O ions, respectively. Generally, the most stable structure is tetragonal for  $t \gtrsim 1$ , cubic for  $t \approx 1$ , and rhombohedral or orthorhombic for  $t \lesssim 1$ . In fact,  $\text{BaTiO}_3$  ( $t = 1.062$ ) and  $\text{SrTiO}_3$  ( $t = 1.002$ ) show tetragonal and cubic structures in room temperature, respectively. However, under external pressure, e.g., hydrostatic or in-plane pressure (Ahart *et al.*, 2008; Fujii *et al.*, 1987; Haeni *et al.*, 2004), the most stable structures of  $\text{ABO}_3$  generally change; e.g.,  $\text{SrTiO}_3$  shows the tetragonal and ferroelectric structure even in room temperature when the  $a$  lattice parameter along the [100] axis (and also the [010] axis) is smaller than the bulk lattice parameter with compressive stress (Haeni *et al.*, 2004). Theoretical investigations of ferroelectric  $\text{ABO}_3$  under hydrostatic or in-plane pressure by first-principles calculations have been reported (Bévilion *et al.*, 2007; Diéguez *et al.*, 2005; Furuta & Miura, 2010; Khenata *et al.*, 2005; Kornev *et al.*, 2005; Miura *et al.*, 2010a; Ricinschi *et al.*, 2006; Uratani *et al.*, 2008; Z. Wu *et al.*, 2005), and their calculated results are consistent with the experimental results. However, even in  $\text{BaTiO}_3$ , which are a well-known lead-free ferroelectric and piezoelectric  $\text{ABO}_3$ , few theoretical papers about the piezoelectric properties with in-plane compressive stress have been reported.

Recently, we investigated the roles of the Ti–O Coulomb repulsions in the appearance of a ferroelectric states in tetragonal  $\text{BaTiO}_3$  by the analysis of a first-principles PP method (Miura *et al.*, 2010a). We investigated the structural properties of tetragonal and rhombohedral  $\text{BaTiO}_3$  with two kind of Ti PPs, and propose the role of Ti 3s and 3p states for ferroelectricity. Moreover, we also investigated the structural, ferroelectric, and piezoelectric properties of tetragonal  $\text{BaTiO}_3$  and  $\text{SrTiO}_3$  with in-plane compressive structures (Furuta & Miura, 2010). We discussed the difference in the piezoelectric mechanisms between  $\text{BaTiO}_3$  and  $\text{SrTiO}_3$  with in-plane compressive structures, which would be important for piezoelectric material design. In this chapter, based on our previous reports (Furuta & Miura, 2010; Miura *et al.*, 2010a), the author discusses a general role of B–O Coulomb repulsions for ferroelectricity and piezoelectricity in  $\text{ABO}_3$ , especially in  $\text{BaTiO}_3$  and  $\text{SrTiO}_3$ .

## 2. Calculations

Calculations of  $\text{BaTiO}_3$  and  $\text{SrTiO}_3$  were performed using the ABINIT package code (Gonze *et al.*, 2002), which is one of the norm-conserving PP (NCPP) methods. Electron-electron interaction was treated in the local-density approximation (LDA) (Perdew & Wang, 1992). Pseudopotentials were generated using the OPIUM code (Rappe, 2004):

(i) In order to investigate the role of Ti 3s and 3p states for  $\text{BaTiO}_3$ , two kinds of Ti PPs were prepared: one is the Ti PP with 3s, 3p, 3d and 4s electrons treated as semicore or valence electrons (Ti3spd4s PP), and the other is the Ti PP with only 3d and 4s electrons treated as valence electrons (Ti3d4s PP). The above pseudopotentials were generated using the OPIUM

code (Rappe, 2004), and the differences between the calculated result and the experimental one are within 1.5 % of the lattice parameter and within 10 % of the bulk modulus in the optimized calculation of bulk Ti in both PPs. Moreover, Ba PP with 5s, 5p and 6s electrons treated as semicore or valence electrons, and O PP with 2s and 2p electrons treated as semicore or valence electrons, were also prepared. The cutoff energy for plane-wave basis functions was set to be 50 Hartree (Hr). A  $6 \times 6 \times 6$  Monkhorst-Pack  $k$ -point mesh was set in the Brillouin zone of the unit cell. The number of atoms in the unit cell was set to be five, and positions of all the atoms were optimized within the framework of the tetragonal ( $P4mm$ ) or rhombohedral ( $R3m$ ) structure.

(ii) The ferroelectric and piezoelectric properties of  $SrTiO_3$  and  $BaTiO_3$  with compressive tetragonal structures are investigated. Pseudopotentials were generated using the OPIUM code (Rappe, 2004); 4s (5s), 4p (5p) and 5s (6s) electrons for Sr (Ba), 3s, 3p, 3d and 4s electrons for Ti, and 2s and 2p electrons for O were treated as semicore or valence electrons. The cutoff energy for the plane wave basis functions was set to be 50 Hr. A  $6 \times 6 \times 6$  Monkhorst-Pack  $k$ -point mesh was set in the Brillouin zone of the unit cell. The number of atoms in the  $ABO_3$  unit cell was set to be five, and the coordinations of all the atoms were optimized within a framework of the tetragonal ( $P4mm$ ) structure. An  $6 \times 6 \times 6$  Monkhorst-Pack  $k$ -point sampling was set in Brillouin zone of the unit cell.

In the present calculations, spontaneous polarizations and piezoelectric constants were also evaluated, due to the Born effective charges (Resta, 1994) and density-functional perturbation theory (Hamann et al., 2005; X. Wu et al., 2005). The spontaneous polarization of tetragonal structures along the [001] axis,  $P_3$ , is defined as,

$$P_3 \equiv \sum_k \frac{ec}{\Omega} Z_{33}^*(k) u_3(k), \quad (2)$$

where  $e$ ,  $c$ , and  $\Omega$  denote the charge unit, the lattice parameter of the unit cell along the [001] axis, and the volume of the unit cell, respectively.  $u_3(k)$  denotes the displacement along the [001] axis of the  $k$ th atom, and  $Z_{33}^*(k)$  denotes the Born effective charges (Resta, 1994) which contributes to the  $P_3$  from the  $u_3(k)$ . The piezoelectric  $e$  constants, on the other hand, are defined as

$$e_{\alpha\beta} \equiv \left( \frac{\partial P_\alpha}{\partial \eta_\beta} \right)_u + \sum_k \left( \frac{\partial P_\alpha}{\partial u_\alpha(k)} \right)_\eta \frac{\partial u_\alpha(k)}{\partial \eta_\beta}, \quad (3)$$

where  $P$ ,  $\eta$ , and  $u(k)$  denote the spontaneous polarization, the strain, and the displacement of the  $k$ th atom, respectively.  $\alpha$  and  $\beta$  denote the direction-indexes of the axis, i.e., 1 along the [100] axis, 2 along the [010] axis, and 3 along the [001] axis, respectively. In eq. (3), the first term of the right hand denotes the clamped term evaluated at vanishing internal strain, and the second term denotes the relaxed term that is due to the relative displacements. According to the eqs. (2) and (3), therefore,  $e_{33}$  or  $e_{31}$  can be especially written as,

$$e_{3\beta} = \left( \frac{\partial P_3}{\partial \eta_\beta} \right)_u + \sum_k \frac{ec}{\Omega} Z_{33}^*(k) \frac{\partial u_3(k)}{\partial \eta_\beta} \quad (\beta = 3, 1). \quad (4)$$

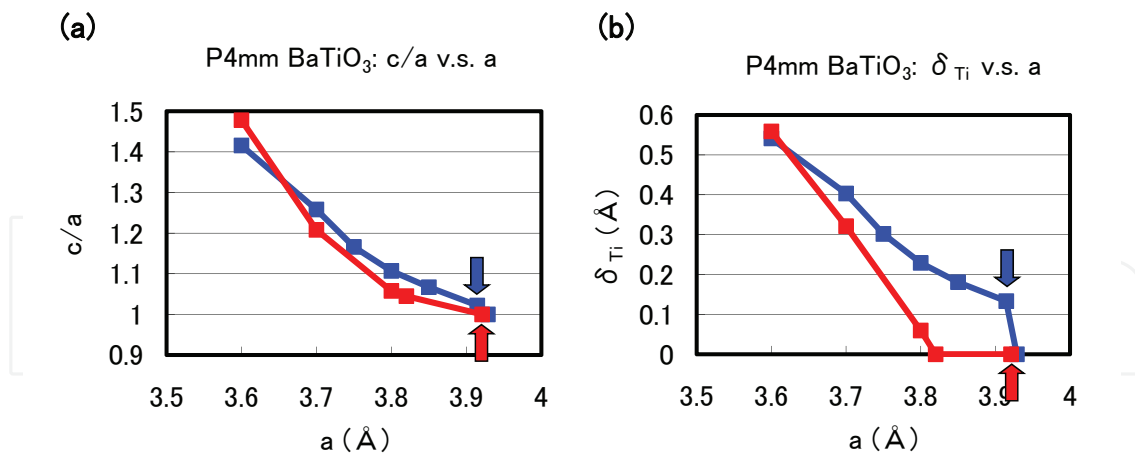


Fig. 1. Optimized calculated results as a function of  $a$  lattice parameters in tetragonal BaTiO<sub>3</sub>: (a)  $c/a$  ratio and (b)  $\delta_{Ti}$  to the [001] axis. Blue lines correspond to the results with the Ti3spd4s PP, and red lines correspond to those with the Ti3d4s PP. Results with arrows are the fully optimized results, and the other results are those with  $c$  and all the inner coordinations optimized for fixed  $a$  (Miura et al., 2010a).

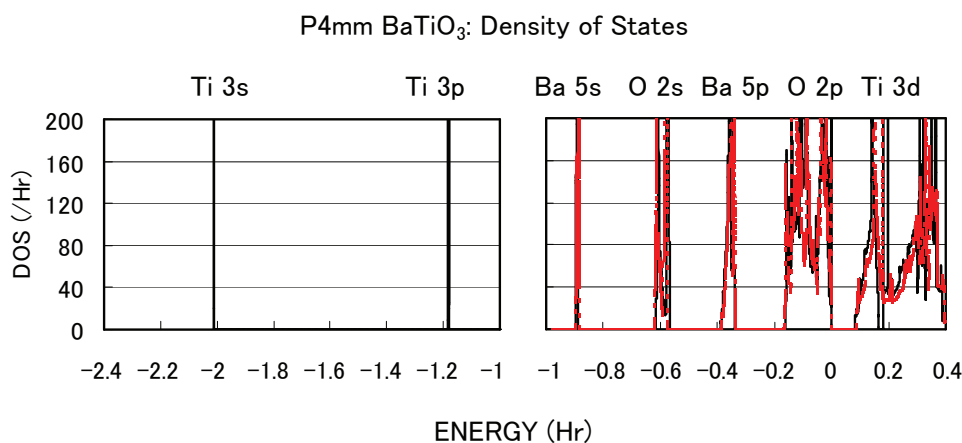


Fig. 2. Total density of states (DOS) of fully optimized tetragonal BaTiO<sub>3</sub> with the Ti3spd4s PP (solid line) and cubic BaTiO<sub>3</sub> with the Ti3d4s PP (red dashed line) (Miura et al., 2010a).

### 3. Results and discussion

#### 3.1 BaTiO<sub>3</sub>: Role of Ti 3s and 3p states for ferroelectricity

In this subsection, the author discusses the role of Ti 3s and 3p states for ferroelectricity for ferroelectricity in tetragonal BaTiO<sub>3</sub>.

Figures 1(a) and 1(b) show the optimized results for the ratio  $c/a$  of the lattice parameters and the value of the Ti ion displacement ( $\delta_{Ti}$ ) as a function of the  $a$  lattice parameters in tetragonal BaTiO<sub>3</sub>, respectively. Results with arrows are the fully optimized results, and the others results are those with the  $c$  lattice parameters and all the inner coordinations optimized for fixed

a. Note that the fully optimized structure of  $BaTiO_3$  is tetragonal with the  $Ti3spd4s$  PP, whereas it is cubic ( $Pm\bar{3}m$ ) with the  $Ti3d4s$  PP. As shown in Fig. 1(a) and 1(b),  $c/a$  and  $\delta_{Ti}$  show significantly different results for  $a \gtrsim 3.7$  whereas they show almost the same results for  $a \lesssim 3.7$ , for both Ti PPs. This result suggests that the optimized results of  $ABO_3$  with smaller lattice parameters, e.g., under high pressure (Bévilion et al., 2007), are almost independent of the choice of PP.

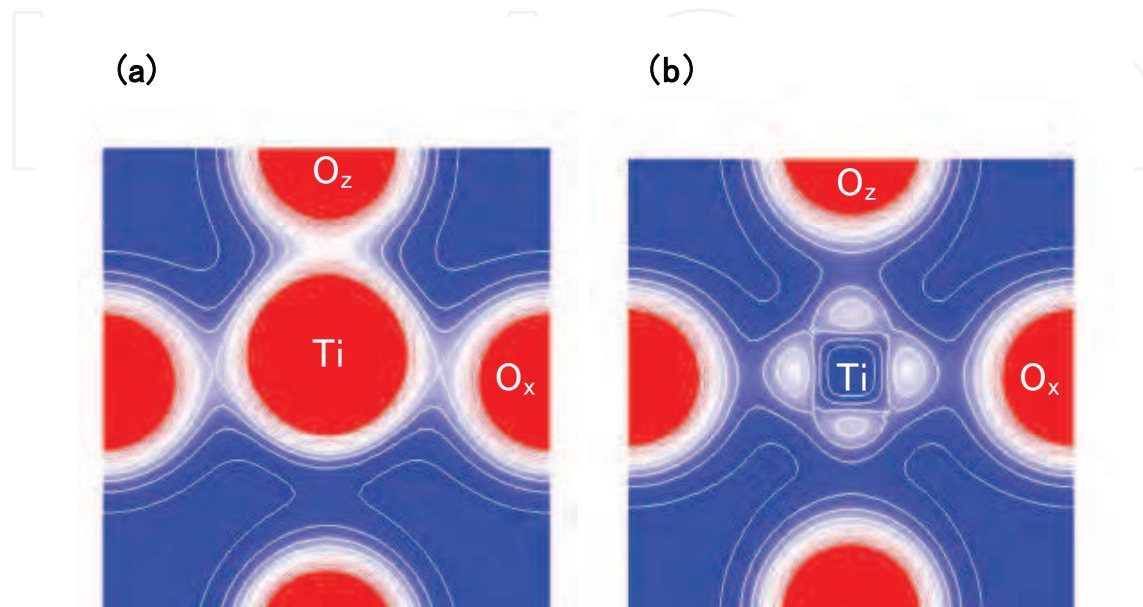


Fig. 3. Two-dimensional electron-density contour map on the  $xz$ -plane for tetragonal  $BaTiO_3$ : (a) with the  $Ti3spd4s$  PP, and (b) with the  $Ti3d4s$  PP. The optimized calculated results with  $a$  fixed to be 3.8 are shown in both figures. The electron density increases as color changes from blue to red via white. Contour curves are drawn from  $0.4$  to  $2.0 e^3$  with increments of  $0.2 e^3$  (Miura et al., 2010a).

The calculated results shown in Fig. 1 suggest that the explicit treatment of Ti 3s and 3p semicore states is essential to the appearance of ferroelectric states in  $BaTiO_3$ . In the following, the author investigates the role of Ti 3s and 3p states for ferroelectricity from two viewpoints. One viewpoint concerns hybridizations between Ti 3s and 3p states and other states. Figure 2 shows the total density of states (DOS) of tetragonal  $BaTiO_3$  with two Ti PPs. Both results are in good agreement with previous calculated results (Chen et al., 2004; Khenata et al., 2005) by the full-potential linear augmented plane wave (FLAPW) method. In the DOS with the  $Ti3spd4s$  PP, the energy “levels”, not bands, of Ti 3s and 3p states, are located at  $-2.0$  Hr and  $-1.2$  Hr, respectively. This result suggests that the Ti 3s and 3p orbitals do not make any hybridizations but only give Coulomb repulsions with the O orbitals as well as the Ba orbitals. In the DOS with the  $Ti3d4s$  PP, on the other hand, the energy levels of Ti 3s and 3p states are not shown because Ti 3s and 3p states were treated as the core charges. This result means that the Ti 3s and 3p orbitals cannot even give Coulomb repulsions with the O orbitals as well as the Ba orbitals.

Another viewpoint is about the Coulomb repulsions between Ti 3s and  $3p_{x(y)}$  states and  $O_{x(y)}$  2s and  $2p_{x(y)}$  states in tetragonal  $BaTiO_3$ . Figures 3(a) and 3(b) show two-dimensional electron-density contour map on the  $xz$ -plane for tetragonal  $BaTiO_3$  with the  $Ti3spd4s$  PP, and that with the  $Ti3d4s$  PP, respectively. These are the optimized calculated results with  $a$  fixed

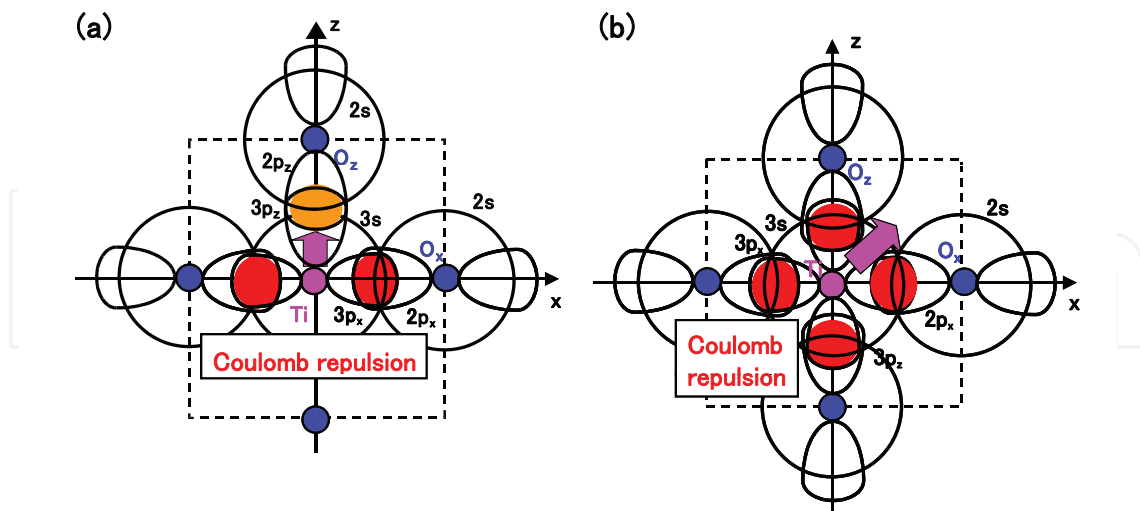


Fig. 4. Illustrations of the proposed mechanisms for the Coulomb repulsions between Ti 3s and 3p states and O 2s and 2p states in BaTiO<sub>3</sub>: (a) anisotropic Coulomb repulsions between Ti 3s and 3p<sub>x(y)</sub> states and O<sub>x(y)</sub> 2s and 2p<sub>x(y)</sub> states, and between Ti 3s and 3p<sub>z</sub> states and O<sub>z</sub> 2s and 2p<sub>z</sub> states, in the tetragonal structure. (b) isotropic Coulomb repulsions between Ti 3s and 3p<sub>x(y)(z)</sub> states and O<sub>x(y)(z)</sub> 2s and 2p<sub>x(y)(z)</sub> states, in the rhombohedral structure (Miura et al., 2010a).

to be 3.8, and the electron density in Fig. 3(a) is quantitatively in good agreement with the experimental result (Kuroiwa et al., 2001). The electron density between Ti and O<sub>x</sub> ions in Fig. 3(a) is larger than that in Fig. 3(b), which suggests that Ti ion displacement is closely related to the Coulomb repulsions between Ti 3s and 3p states and O 2s and 2p states along the [001] axis (the z-axis in this case).

The present discussion of the Coulomb repulsions is consistent with the previous reports. A recent soft mode investigation (Oguchi et al., 2009) of BaTiO<sub>3</sub> shows that Ba ions contribute little to the appearance of Ti ion displacement along the [001] axis. This result suggests that Ti ion displacement is closely related to the structural distortion of TiO<sub>6</sub> octahedra. In the present calculations, on the other hand, the only difference between BaTiO<sub>3</sub> with the Ti3spd4s PP and with the Ti3d4s PP is the difference in the expression for the Ti 3s and 3p states, i.e., the explicit treatment and including core charges. However, our previous calculation (Miura & Tanaka, 1998) shows that the strong Coulomb repulsions between Ti 3s and 3p<sub>z</sub> states and O<sub>z</sub> 2s and 2p<sub>z</sub> states do not favour Ti ion displacement along the [001] axis. This result suggests that the Coulomb repulsions between Ti 3s and 3p<sub>x(y)</sub> states and O<sub>x(y)</sub> 2s and 2p<sub>x(y)</sub> states would contribute to Ti ion displacement along the [001] axis, and the suggestion is consistent with a recent calculation (Uratani et al., 2008) for PbTiO<sub>3</sub> indicating that the tetragonal and ferroelectric structure appears more favourable as the *a* lattice parameter decreases.

Considering the above investigations, the author proposes the mechanism of Ti ion displacement as follows: Ti ion displacement along the z-axis appears when the Coulomb repulsions between Ti 3s and 3p<sub>x(y)</sub> states and O<sub>x(y)</sub> 2s and 2p<sub>x(y)</sub> states, in addition to the dipole-dipole interaction, overcome the Coulomb repulsions between Ti 3s and 3p<sub>z</sub> states and O<sub>z</sub> 2s and 2p<sub>z</sub> states (Miura & Tanaka, 1998). An illustration of the Coulomb repulsions is shown in Fig. 4(a). In fully optimized BaTiO<sub>3</sub> with the Ti3spd4s PP, the Ti ion can be displaced due to the above mechanism. In fully optimized BaTiO<sub>3</sub> with the Ti3d4s PP, on the other

hand, the Ti ion cannot be displaced due to the weaker Coulomb repulsions between Ti and  $O_{x(y)}$  ions. However, since the Coulomb repulsion between Ti and  $O_z$  ions in  $BaTiO_3$  with the Ti3d4s PP is also weaker than that in  $BaTiO_3$  with the Ti3spd4s PP, the Coulomb repulsions between between Ti and  $O_{x(y)}$  ions in addition to the log-range force become comparable to the Coulomb repulsions between Ti and  $O_z$  ions both in Ti PPs, as the lattice parameter  $a$  becomes smaller. The above discussion suggests that the hybridization between Ti 3d and  $O_z$  2s and  $2p_z$  stabilizes Ti ion displacement, but contribute little to a driving force for the appearance of Ti ion displacement.

It seems that the above proposed mechanism for tetragonal  $BaTiO_3$  can be applied to the mechanism of Ti ion displacement in rhombohedral  $BaTiO_3$ , as illustrated in Fig. 4(b). The strong isotropic Coulomb repulsions between Ti 3s and  $3p_{x(y)(z)}$  states and  $O_{x(y)(z)}$  2s and  $2p_{x(y)(z)}$  states yield Ti ion displacement along the [111] axis. On the other hand, when the isotropic Coulomb repulsions are weaker or stronger, the Ti ion cannot be displaced and therefore it is favoured for the crystal structure to be cubic.

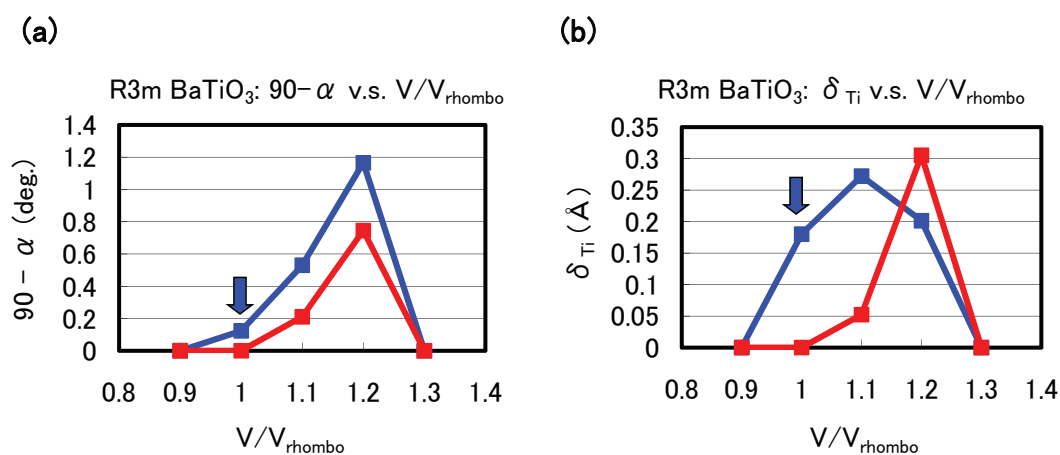


Fig. 5. Optimized calculated results as a function of the fixed volumes of the unit cells in rhombohedral  $BaTiO_3$ : (a)  $90 - \alpha$  degree and (b)  $\delta_{\text{Ti}}$  to the [111] axis. Blue lines correspond to the results with the Ti3spd4s PP, and red lines correspond to those with the Ti3d4s PP.  $V_{\text{rhombo}}$  denote the volume of the fully optimized unit cell with the Ti 3spd4s PP. Results with arrows are the fully optimized results, and the other results are those with all the inner coordinations optimized for fixed volumes of the unit cells (Miura et al., 2010a).

Let us investigate the structural properties of rhombohedral  $BaTiO_3$ . Figures 5(a) and 5(b) show the optimized results of the  $90 - \alpha$  degree and  $\delta_{\text{Ti}}$  as a function of fixed volumes of the unit cells in rhombohedral  $BaTiO_3$ , respectively, where  $\alpha$  denotes the angle between two lattice vectors. In these figures,  $\alpha$  denotes the angle between two crystal axes of rhombohedral  $BaTiO_3$ , and  $\delta_{\text{Ti}}$  denotes the value of the Ti ion displacement along the [111] axis. Results with arrows are the fully optimized results;  $V_{\text{rhombo}}$  denote the volume of the fully optimized unit cell with the Ti 3spd4s PP. The other results are those with all the inner coordinations optimized with fixed volumes of the unit cells. The proposal mechanisms about the Coulomb repulsions seem to be consistent with the calculated results shown in Fig. 5: For  $V/V_{\text{rhombo}} \lesssim 0.9$  or  $\gtrsim 1.3$ , the isotropic Coulomb repulsions are weaker or stronger, and the Ti ion cannot be displaced along the [111] axis and therefore the crystal structure is cubic for both Ti PPs. For  $0.9 \lesssim V/V_{\text{rhombo}} \lesssim 1.3$ , on the other hand, the isotropic Coulomb repulsions



are strong enough to yield Ti ion displacement for both Ti PPs. However, since the magnitude of the isotropic Coulomb repulsion is different in the two Ti PPs, the properties of the  $90-\alpha$  degree and  $\delta_{\text{Ti}}$  are different quantitatively.

### 3.2 Role of the Ti–O Coulomb repulsions for piezoelectric SrTiO<sub>3</sub> and BaTiO<sub>3</sub>

As discussed in the previous subsection, the Coulomb repulsions between Ti 3s and  $3p_{x(y)}$  states and  $O_{x(y)}$  2s and  $2p_{x(y)}$  states have an important role in the appearance of the ferroelectric state in tetragonal BaTiO<sub>3</sub>. In this subsection, the author discusses the role of the Ti–O Coulomb repulsions for piezoelectric SrTiO<sub>3</sub> and BaTiO<sub>3</sub>.

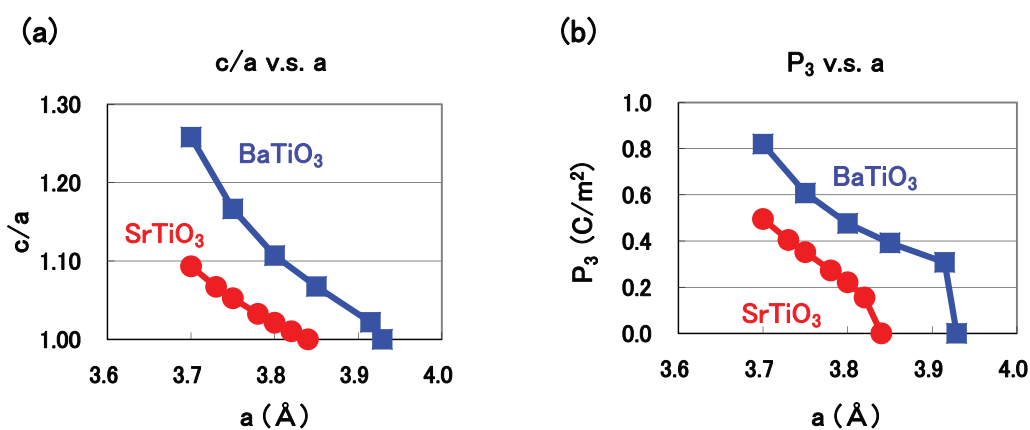


Fig. 6. Optimized calculated results as a function of  $a$  lattice parameters in compressive tetragonal SrTiO<sub>3</sub> and BaTiO<sub>3</sub>: (a)  $c/a$  ratio and (b)  $P_3$ , i.e., spontaneous polarization along the [001] axis (Furuta & Miura, 2010).

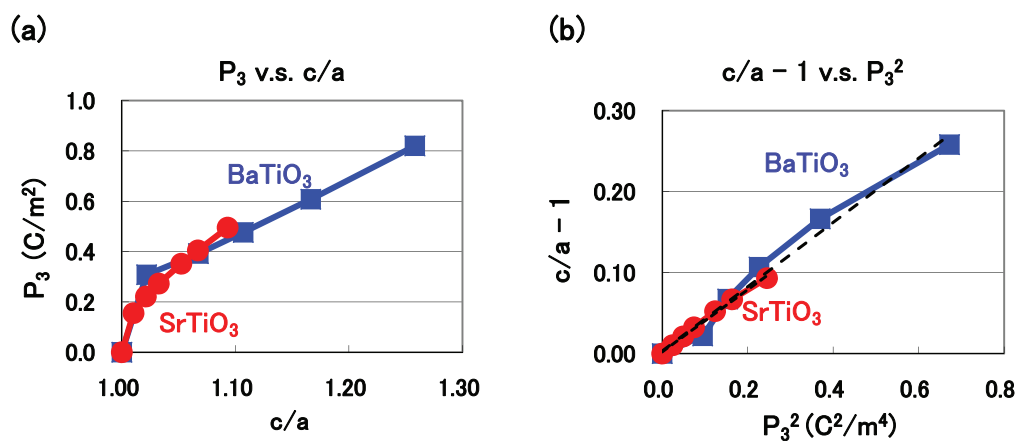


Fig. 7. (a)  $P_3$  as a function of  $c/a$  ratios, and (b)  $c/a$  ratio as a function of  $P_3^2$ . These values are derived from the calculated results as shown in Figs. 6(a) and (b). Dotted and dashed lines in Fig. 7(b) serve as visual guides for SrTiO<sub>3</sub> and BaTiO<sub>3</sub>, respectively (Furuta & Miura, 2010).

Figures 6(a) shows the optimized results for the ratio  $c/a$  as a function of the  $a$  lattice parameters in tetragonal SrTiO<sub>3</sub> and BaTiO<sub>3</sub>. These results are the fully optimized results and the results with the  $c$  lattice parameters and all the inner coordinations optimized for

fixed  $a$ . The fully optimized parameters of  $SrTiO_3$  ( $a = 3.84$  : cubic) and  $BaTiO_3$  ( $a = 3.91$  and  $c = 4.00$  : tetragonal) are within 2.0% in agreement with the experimental results in room temperature. Figure 6(b) shows the evaluated results for  $P_3$  as a function of the  $a$  lattice parameters in tetragonal  $SrTiO_3$  and  $BaTiO_3$ , where  $P_3$ , which is evaluated by eq. (2), denotes the spontaneous polarization along the [001] axis. Note that the tetragonal and ferroelectric structures appear even in  $SrTiO_3$  when the fixed  $a$  lattice parameter is compressed to be smaller than the fully-optimized  $a$  lattice parameter. As shown in Figs. 6(a) and 6(b), the tetragonal and ferroelectric structure appear more favorable as the fixed  $a$  lattice parameter decreases, which is consistent with previous calculated results (Miura et al., 2010a; Ricinchi et al., 2006; Uratani et al., 2008). The results would be due to the suggestion discussed in the previous section that the large Coulomb repulsion of  $Ti$ - $O$  bondings along the [100] axis (and the [010] axis) is a driving force of the displacement of  $Ti$  ions along the [001] axis, i.e., the large Coulomb repulsion along the [100] axis (and the [010] axis) is essential for the appearance of the tetragonal structure. Figure 7(a) shows the relationship between  $P_3$  and the ratio  $c/a$ , where  $P_3$  and  $c/a$  are derived from the calculated results shown in Figs. 6(a) and 6(b). The property of  $BaTiO_3$  in Fig. 7(a) is in qualitatively agreement with a previous calculational result (Ricinchi et al., 2006). Figure 7(b) shows the relationship between the ratio  $c/a$  and  $P_3^2$ . Note that  $c/a - 1$  is proportional to  $P_3^2$  with almost the same coefficients in both  $SrTiO_3$  and  $BaTiO_3$ . Clearly, the ratio  $c/a$  is a good parameter in both tetragonal  $SrTiO_3$  and  $BaTiO_3$  with in-plane compressive stress. Therefore, in the following, the author uses the ratio  $c/a$  as a parameter for the investigations of the piezoelectric properties.

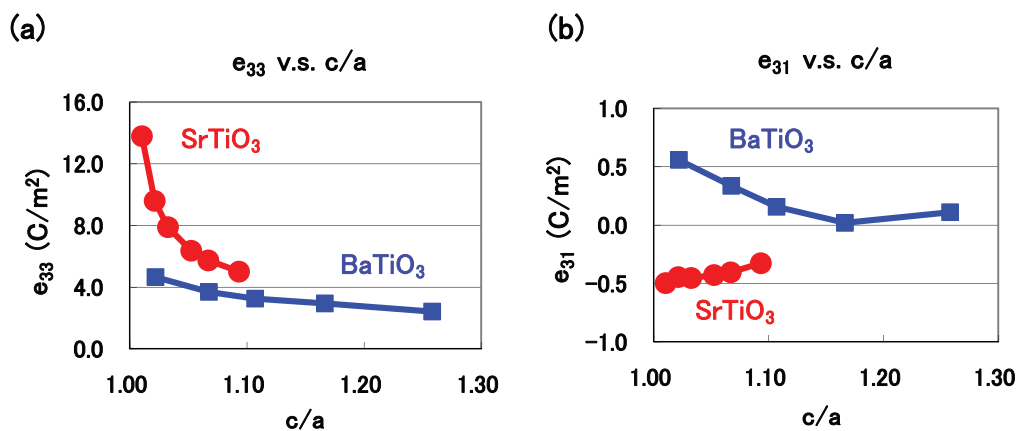


Fig. 8. Evaluated piezoelectric constants as a function of  $c/a$  ratios in optimized tetragonal  $SrTiO_3$  and  $BaTiO_3$ : (a)  $e_{33}$  and (b)  $e_{31}$  (Furuta & Miura, 2010).

Figures 8(a) and 8(b) shows the piezoelectric properties of  $e_{33}$  and  $e_{31}$  as a function of the ratio  $c/a$  in tetragonal  $SrTiO_3$  and  $BaTiO_3$ . The ratio  $c/a$  is optimized value as shown in Fig. 6(a) and  $e_{33}$  and  $e_{31}$  are evaluated values in their optimized structures. Note that  $e_{33}$  become larger at  $c/a \approx 1$ , especially in  $SrTiO_3$ . These properties seem to be similar to the properties around the Curie temperatures in piezoelectric  $ABO_3$ ; Damjanovic emphasized the importance of the polarization extension as a mechanism of larger piezoelectric constants in a recent paper (Damjanovic, 2010). Contrary to  $e_{33}$ , on the other hand, the changes in  $e_{31}$  are much smaller than the changes in  $e_{33}$ , but note that  $e_{31}$  shows negative in  $SrTiO_3$  while positive in  $BaTiO_3$ .

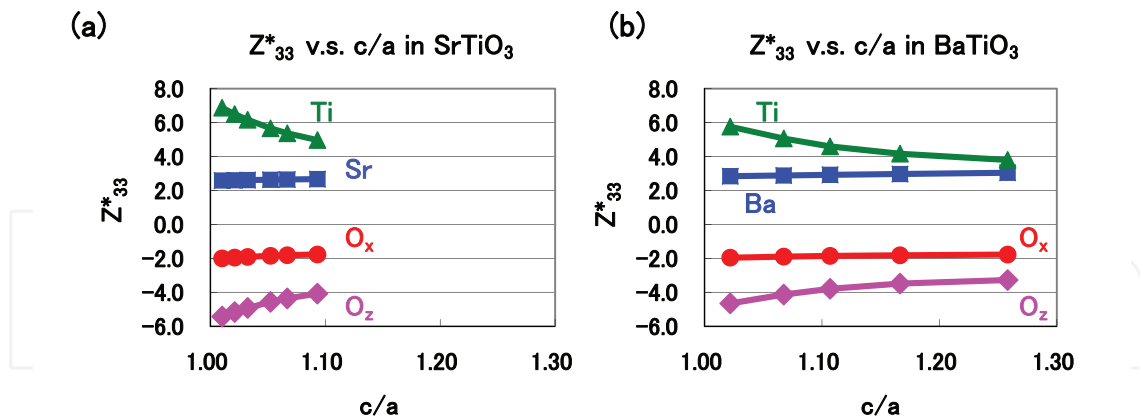


Fig. 9. Evaluated Born effective charges  $Z_{33}^*(k)$  as a function of  $c/a$  ratios: (a) SrTiO<sub>3</sub> and (b) BaTiO<sub>3</sub>. O<sub>x</sub> and O<sub>z</sub> denote oxygen atoms along the [100] axis and the [001] axis, respectively (Furuta & Miura, 2010).

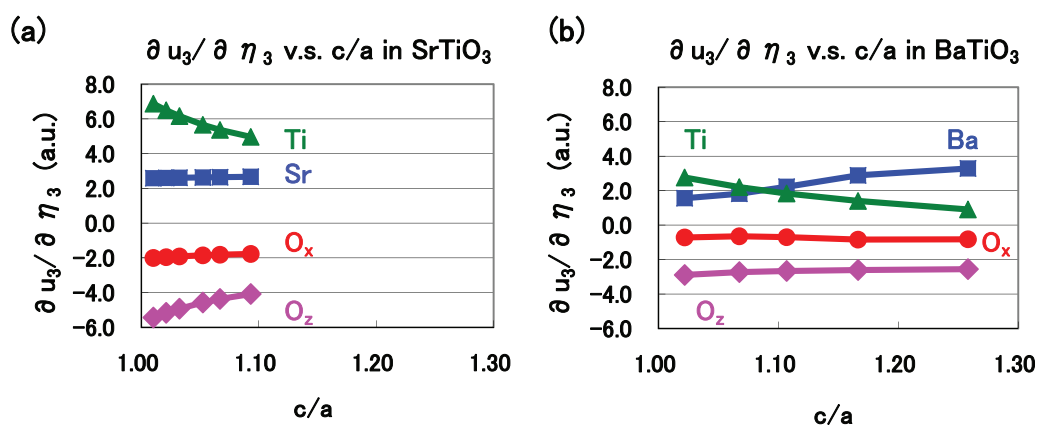


Fig. 10. Evaluated values of  $\partial u_3(k) / \partial \eta_3$  as a function of  $c/a$  ratios: (a) SrTiO<sub>3</sub> and (b) BaTiO<sub>3</sub>. "a.u." denotes the atomic unit ( $\approx 0.53$ ) (Furuta & Miura, 2010).

As expressed in eq. (4),  $e_{3j}$  is the sum of the contributions from the clamped term and the relaxed term. However, it has been generally known that the contribution to  $e_{3j}$  from the clamped term is much smaller than that from the relaxed term; in fact, the absolute values of the  $e_{33}$  clamped terms are less than  $1 \text{ C/m}^2$  in both SrTiO<sub>3</sub> and BaTiO<sub>3</sub>. The author therefore investigates the contributions to the relaxed term of  $e_{33}$  and  $e_{31}$  in detail. As expressed in eq. (4), the relaxed terms of  $e_{3j}$  are proportional to the sum of the products between the  $Z_{33}^*(k)$  and  $\partial u_3(k) / \partial \eta_j$  ( $j = 3$  or  $1$ ) values. Let us show the evaluated results of  $Z_{33}^*(k)$ ,  $\partial u_3(k) / \partial \eta_3$ , and  $\partial u_3(k) / \partial \eta_1$  in the following. Figures 9(a) and 9(b) show the  $Z_{33}^*(k)$  values in SrTiO<sub>3</sub> and BaTiO<sub>3</sub>, respectively. Properties of the  $Z_{33}^*(k)$  values are quantitatively similar in both SrTiO<sub>3</sub> and BaTiO<sub>3</sub>. Therefore, the difference in the properties of  $e_{33}$  and  $e_{31}$  between SrTiO<sub>3</sub> and BaTiO<sub>3</sub> must be due to the difference in the properties of  $\partial u_3(k) / \partial \eta_j$ . Figures 10(a) and 10(b) show the  $\partial u_3(k) / \partial \eta_3$  values in SrTiO<sub>3</sub> and BaTiO<sub>3</sub>, respectively. In these figures, O<sub>x</sub> and O<sub>z</sub> denote oxygen atoms along the [100] and [001] axes, respectively, and  $\eta_3$  is defined as  $\eta_3 \equiv (c - c_0) / c_0$ , where  $c_0$  denotes the  $c$  lattice parameter with fully optimized structure. Clearly, the absolute values of  $\partial u_3(k) / \partial \eta_3$  are different in between SrTiO<sub>3</sub> and BaTiO<sub>3</sub>. On

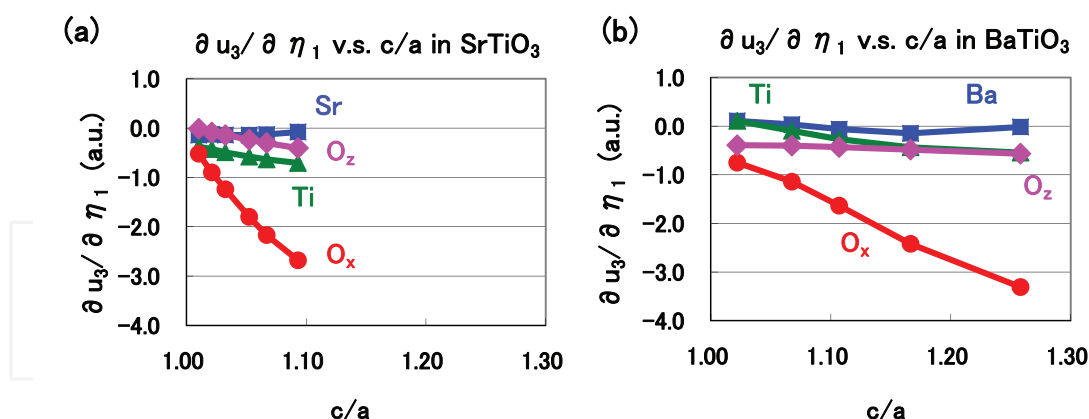


Fig. 11. Evaluated values of  $\partial u_3(k)/\partial \eta_1$  as a function of  $c/a$  ratios: (a)  $SrTiO_3$  and (b)  $BaTiO_3$  (Furuta & Miura, 2010).

the other hand, Figs. 11(a) and 11(b) show the  $\partial u_3(k)/\partial \eta_1$  values in  $SrTiO_3$  and  $BaTiO_3$ , respectively;  $\eta_1$  is defined as  $\eta_1 \equiv (a - a_0)/a_0$ , where  $a_0$  denotes the  $a$  lattice parameter with fully optimized structure. The absolute values of  $\partial u_3(k)/\partial \eta_1$ , especially for Ti,  $O_x$ , and  $O_z$ , are different in between  $SrTiO_3$  and  $BaTiO_3$ . As a result, the quantitative differences in  $e_{33}$  and  $e_{31}$  in between  $SrTiO_3$  and  $BaTiO_3$  are due to the differences in the contribution of the  $\partial u_3(k)/\partial \eta_j$  values. In the following, the author would like to discuss the reasons of the quantitative differences in  $e_{33}$  and  $e_{31}$  in between  $SrTiO_3$  and  $BaTiO_3$ .

Figure 12(a) shows the difference between the  $A-O_x$  distance ( $R_{A-O_x}$ ) and the sum of  $r_A$  and  $r_{O_x}$  ( $r_A + r_{O_x}$ ) on the (100) plane as a function of the ratio  $c/a$ , where the values of the ionic radii are defined as Shannon's ones (Shannon, 1976). Note that  $R_{A-O_x}$  is smaller than  $r_A + r_{O_x}$  in both  $SrTiO_3$  and  $BaTiO_3$ . However, the difference in absolute value between  $R_{A-O_x}$  and  $r_A + r_{O_x}$  in  $SrTiO_3$  is much smaller than the difference in  $BaTiO_3$  for  $1.00 \lesssim c/a \lesssim 1.10$ . This result suggests that the  $Sr-O_x$  Coulomb repulsion on the (100) plane in  $SrTiO_3$  is much smaller than the  $Ba-O_x$  Coulomb repulsion in  $BaTiO_3$  and that therefore Sr and  $O_x$  ions of  $SrTiO_3$  can be displaced more easily along the [001] axis than Ba and  $O_x$  ions of  $BaTiO_3$ . This would be a reason why the absolute values of  $\partial u_3(k)/\partial \eta_3$  of Sr and  $O_x$  ions in  $SrTiO_3$  are larger than those of Ba and  $O_x$  ions in  $BaTiO_3$ . Figure 12(b) shows the difference between the  $Ti-O_z$  distance ( $R_{Ti-O_z}$ ) and  $r_{Ti} + r_{O_z}$  along the [001] axis as a function of the ratio  $c/a$ . Note that  $R_{Ti-O_z}$  is smaller than  $r_{Ti} + r_{O_z}$  in both  $SrTiO_3$  and  $BaTiO_3$ . However, the difference in absolute value between  $R_{Ti-O_z}$  and  $r_{Ti} + r_{O_z}$  in  $SrTiO_3$  is smaller than the difference in  $BaTiO_3$  for  $1.00 \lesssim c/a \lesssim 1.10$ . This result suggests that the  $Ti-O_z$  Coulomb repulsion along the [001] axis in  $SrTiO_3$  is smaller than that in  $BaTiO_3$  and that therefore the Ti ion of  $SrTiO_3$  can be displaced more easily along the [001] axis than that of  $BaTiO_3$ . This would be a reason why the absolute values of  $\partial u_3(k)/\partial \eta_3$  of Ti and  $O_z$  ions in  $SrTiO_3$  are larger than that in  $BaTiO_3$ .

In the following, the author discusses the relationship between  $\partial u_3(Ti)/\partial \eta_3$  and the ratio  $c/a$  in detail. Figure 13(a) shows the properties of the differences in the total energy ( $\Delta E_{total}$ ) as a function of  $u_{Ti}$ . In this figure, the properties of  $SrTiO_3$  with  $c/a = 1.021$  ( $\eta = 0.011$ ),  $SrTiO_3$  with  $c/a = 1.093$  ( $\eta = 0.053$ ) and  $BaTiO_3$  with  $c/a = 1.022$  as a reference, are shown. Calculations of  $E_{total}$  were performed with the fixed crystal structures of previously optimized structures except Ti ions. Figure 13(b) shows illustrations of  $\Delta E_{total}$  curves with deviations at the minimum points of the  $\Delta E_{total}$  values, corresponding to the  $\Delta E_{total}$  curves of  $SrTiO_3$  in Fig. 13(a). Clearly, as  $\eta_3$  becomes smaller, the deviated value at the minimum point of the

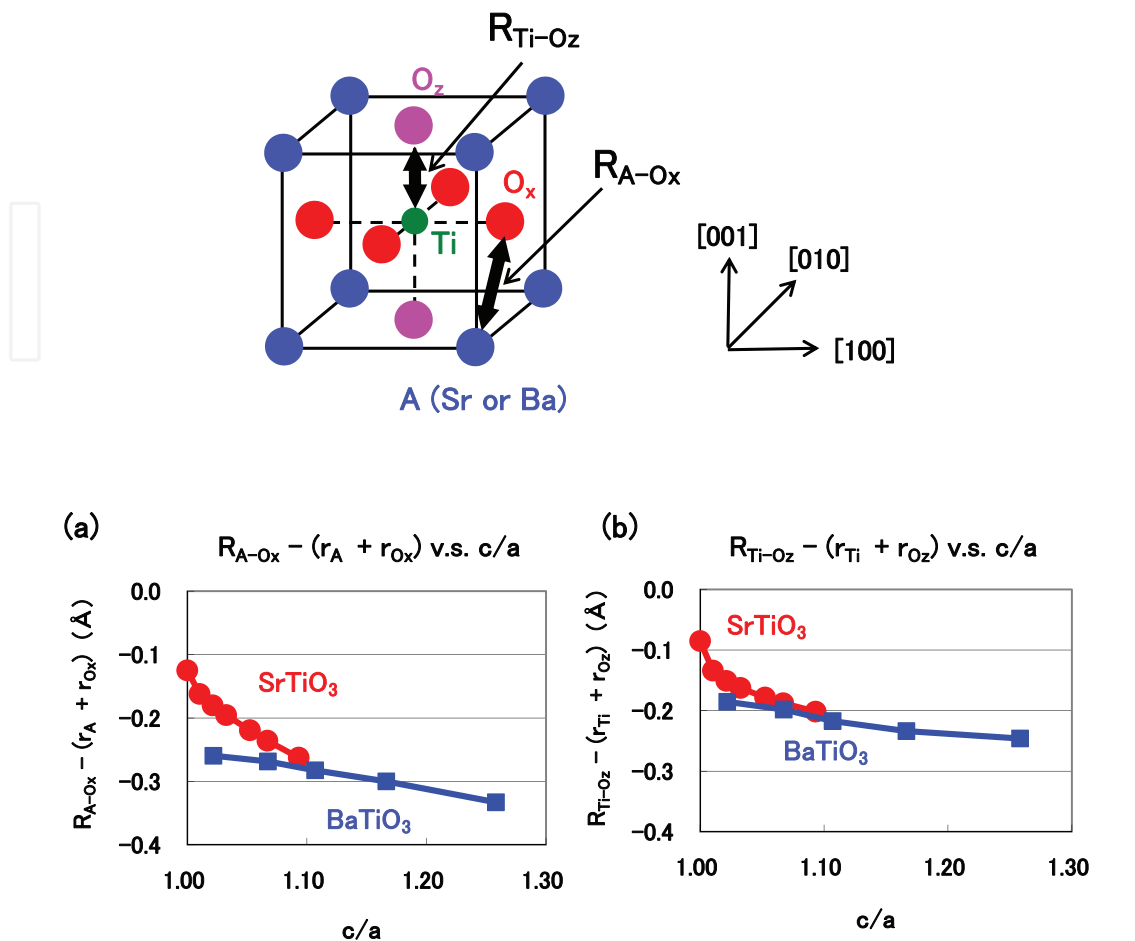


Fig. 12. Evaluated values as a function of  $c/a$  ratios in optimized tetragonal SrTiO<sub>3</sub> and BaTiO<sub>3</sub>: (a) difference between the  $A-O_x$  distance ( $R_{A-O_x}$ ) and  $r_A + r_{O_x}$ , and (b) difference between the  $Ti-O_z$  distance ( $R_{Ti-O_z}$ ) and  $r_{Ti} + r_{O_z}$ , as a function of the ratio  $c/a$ .  $R_{A-O_x}$  and  $R_{Ti-O_z}$  in  $ATiO_3$  are also illustrated; all the ionic radii are much larger, and  $A$  and  $Ti$  ions are displaced along the  $[001]$  axis in real  $ATiO_3$  (Furuta & Miura, 2010).

$\Delta E_{total}$  values becomes smaller, i.e., the  $Ti$  ion can be displaced more favourably. On the other hand, as shown in Fig. 10(a), the absolute value of  $\partial u_3(Ti)/\partial \eta_3$  becomes larger as  $\eta_3$  becomes smaller. Therefore, the  $Ti$  ion can be displaced more favourably as the deviated value at the minimum point of the  $\Delta E_{total}$  values becomes smaller.

Next, let us discuss quantitative properties of  $e_{31}$ , especially the reason why  $e_{31}$  in SrTiO<sub>3</sub> shows negative while positive in BaTiO<sub>3</sub>. Figure 14(a) shows the difference between the  $Ti-O_x$  distance ( $R_{Ti-O_x}$ ) and  $r_{Ti} + r_{O_x}$  along the  $[100]$  axis as a function of the ratio  $c/a$ . Note that  $R_{Ti-O_x}$  is smaller than  $r_{Ti} + r_{O_x}$  in both SrTiO<sub>3</sub> and BaTiO<sub>3</sub>. However, the difference in absolute value between  $R_{Ti-O_x}$  and  $r_{Ti} + r_{O_x}$  in SrTiO<sub>3</sub> is larger than that in BaTiO<sub>3</sub>, i.e.,  $R_{Ti-O_x}$  in SrTiO<sub>3</sub> is smaller than  $R_{Ti-O_x}$  in BaTiO<sub>3</sub>. This result suggests that the  $Ti-O_x$  Coulomb repulsion along the  $[100]$  axis in SrTiO<sub>3</sub> is larger than that in BaTiO<sub>3</sub> and that therefore  $Ti$  and  $O_x$  ions of SrTiO<sub>3</sub> can be displaced along the  $[001]$  axis more easily than those of BaTiO<sub>3</sub>, as discussed in previous subsection. This would be a reason why the absolute values of  $\partial u_3(k)/\partial \eta_1$  of  $Ti$  and  $O_x$  ions in SrTiO<sub>3</sub> are larger than those in BaTiO<sub>3</sub>. Therefore, each

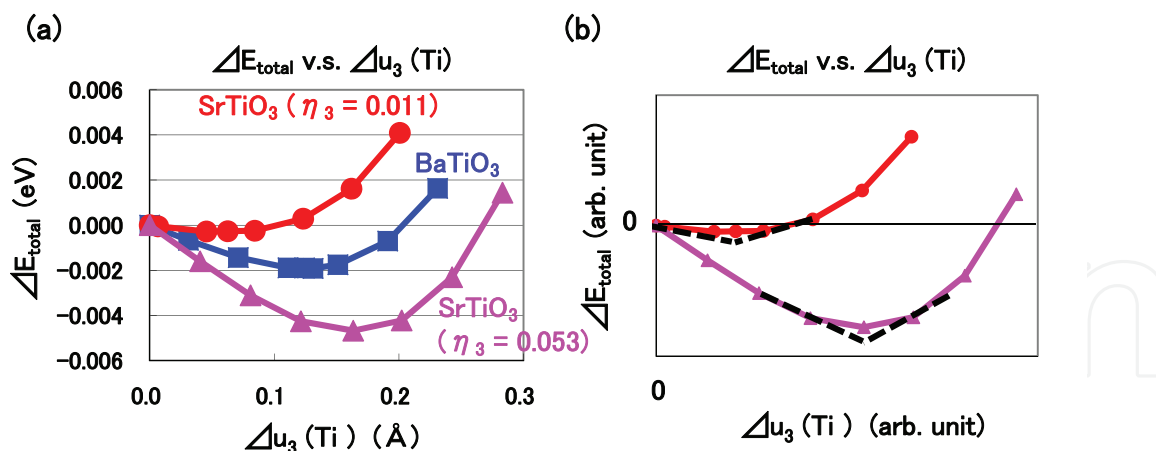


Fig. 13. (a)  $\Delta E_{\text{total}}$  as a function of  $u_{\text{Ti}}$  in tetragonal SrTiO<sub>3</sub> and BaTiO<sub>3</sub>. (b) Illustration of the  $\Delta E_{\text{total}}$  curves in tetragonal SrTiO<sub>3</sub> ( $\eta = 0.011$ ) and SrTiO<sub>3</sub> ( $\eta = 0.053$ ) with deviations at the minimum point of  $\Delta E_{\text{total}}$ .

absolute value of  $Z_{\text{Ti}}^* \times \partial u_3(\text{Ti}) / \partial \eta_1 (< 0)$  and  $Z_{\text{O}_x}^* \times \partial u_3(\text{O}_x) / \partial \eta_1 (> 0)$  in SrTiO<sub>3</sub> is larger than that in BaTiO<sub>3</sub>. Figure 14(b) shows the difference between the  $A\text{--}O_z$  distance ( $R_{A\text{--}O_z}$ ) and  $r_A + r_{O_z}$  on the (001) plane as a function of the ratio  $c/a$ . Note that  $R_{A\text{--}O_z}$  is smaller than  $r_A + r_{O_z}$  in both SrTiO<sub>3</sub> and BaTiO<sub>3</sub>. However, the difference in absolute value between  $R_{A\text{--}O_z}$  and  $r_A + r_{O_z}$  in BaTiO<sub>3</sub> is larger than that in SrTiO<sub>3</sub>. This result suggests that the Ba–O<sub>z</sub> Coulomb repulsion on the (001) plane in BaTiO<sub>3</sub> is larger than that in SrTiO<sub>3</sub> and that therefore O<sub>z</sub> ion of BaTiO<sub>3</sub> can be displaced along the [001] axis more easily than that of SrTiO<sub>3</sub>, as discussed in previous subsection. This would be a reason why the absolute value of  $\partial u_3(k) / \partial \eta_1$  of O<sub>z</sub> ion in BaTiO<sub>3</sub> is larger than that in SrTiO<sub>3</sub>. Therefore, the absolute value of  $Z_{\text{O}_z}^* \times \partial u_3(\text{O}_z) / \partial \eta_1 (> 0)$  in BaTiO<sub>3</sub> is larger than that in SrTiO<sub>3</sub>. Finally, as a result, the above investigations suggest that the signature of  $e_{31}$  in SrTiO<sub>3</sub> or BaTiO<sub>3</sub> is closely related to the difference in absolute values between  $Z_{\text{Ti}}^* \times \partial u_3(\text{Ti}) / \partial \eta_1$  and the sum of  $Z_{\text{O}_x}^* \times \partial u_3(\text{O}_x) / \partial \eta_1$  and  $Z_{\text{O}_z}^* \times \partial u_3(\text{O}_z) / \partial \eta_1$ .

#### 4. Summary

Using a first-principles calculation with optimized structures, the author has investigated the role of the Coulomb repulsions between Ti 3s and 3p states and O 2s and 2p states in ferroelectric BaTiO<sub>3</sub>. It has been found that the Coulomb repulsions between Ti 3s and 3p<sub>x(y)</sub> states and O<sub>x(y)</sub> 2s and 2p<sub>x(y)</sub> states are closely related to the appearance of Ti ion displacement in tetragonal BaTiO<sub>3</sub>. This mechanism seems to be consistent with the appearance of Ti ion displacement in rhombohedral BaTiO<sub>3</sub>. The present investigation suggests that the Coulomb repulsions between Ti 3s and 3p states and O 2p states have an important role in ferroelectricity. In addition to this suggestion, the author believes that the present investigation will show a guideline for the choice of PPs when first-principles calculations with PP methods are performed. The author has also investigated the ferroelectric and piezoelectric properties of SrTiO<sub>3</sub> and BaTiO<sub>3</sub> with in-plane compressive tetragonal structures using a first-principles calculation. It has been found that the ferroelectric structure even in SrTiO<sub>3</sub> appears with in-plane compressive structures. The piezoelectric constant  $e_{33}$  drastically increases in SrTiO<sub>3</sub> rather than that in BaTiO<sub>3</sub> as the tetragonal ratio  $c/a (> 1)$  is

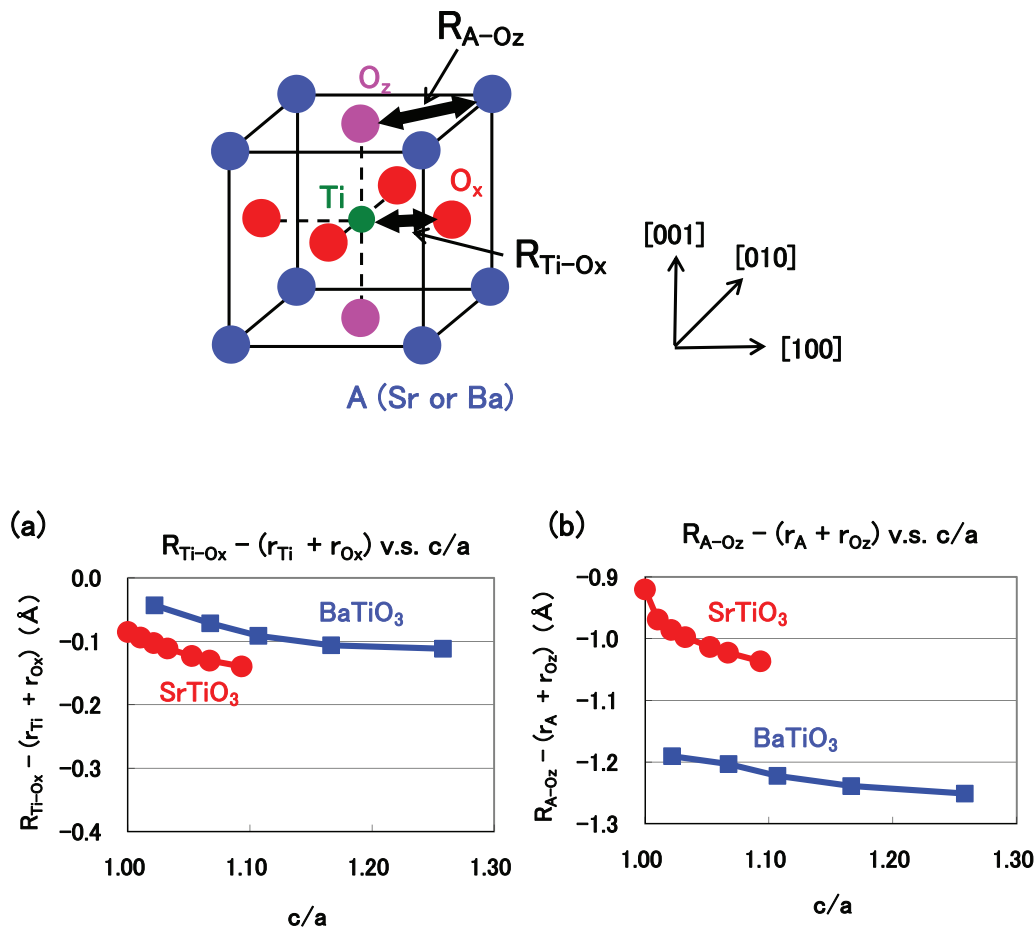


Fig. 14. Evaluated values as a function of  $c/a$  ratios in optimized tetragonal SrTiO<sub>3</sub> and BaTiO<sub>3</sub>: (a) difference between the Ti-O<sub>x</sub> distance ( $R_{Ti-O_x}$ ) and  $r_{Ti} + r_{O_x}$ , as a function of the ratio  $c/a$ , and (b) difference between the A-O<sub>z</sub> distance ( $R_{A-O_z}$ ) and  $r_A + r_{O_z}$ .  $R_{Ti-O_x}$  and  $R_{A-O_z}$  in ATiO<sub>3</sub> are also illustrated (Furuta & Miura, 2010).

close to 1. On the other hand,  $e_{31}$  shows negative in SrTiO<sub>3</sub> while positive in BaTiO<sub>3</sub>, although the changes in their absolute values are very small. The author has found that these properties of  $e_{33}$  and  $e_{31}$  in SrTiO<sub>3</sub> and BaTiO<sub>3</sub> are closely related to the ionic distances.

## 5. Acknowledgements

The author thanks Professor H. Funakubo, Professor M. Azuma, M. Kubota and T. Furuta for useful discussion. The present work was partly supported by the Elements Science and Technology Project from the Ministry of Education, Culture, Sports, Science and Technology, Japan. Calculations for the present work were partly performed by the supercomputing grid cluster machine "TSUBAME" in Tokyo Institute of Technology.

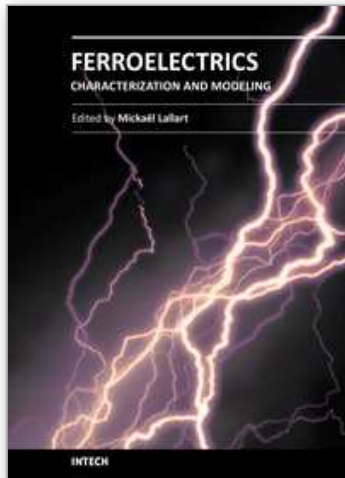
## 6. References

Ahart, M., Somayazulu, M., Cohen, R. E., Ganesh, P., Dera, P., Mao, H., Hemley, R., Ren, Y., Liermann, P. & Wu, Z. (2008). Origin of morphotropic phase boundaries in

- ferroelectrics. *Nature*, Vol. 451, No. 7178, pp. 545-549.
- Bévilion, É. & Geneste, G. (2007). Unstable polar mode and minimum of the dielectric constant in cubic  $BaSnO_3$  under hydrostatic pressure. *Phys. Rev. B*, Vol. 75, No. 21, p. 214106 (5 pages).
- Bousquet, E. & Ghosez, P. (2006). First-principles study of barium titanate under hydrostatic pressure. *Phys. Rev. B*, Vol. 74, No. 18, p. 180101(R) (4 pages).
- Chen, X., Lu, W. & Shen, S. C. (2004). First-principles study of photoconductivity in  $BaTiO_3$  with oxygen vacancies. *Solid State Commun.*, Vol. 130, No. 10, pp. 641-645.
- Cohen, R. E & Krakauer, H. (1990). Lattice dynamics and origin of ferroelectricity in  $BaTiO_3$ : Linearized-augmented-plane-wave total-energy calculations. *Phys. Rev. B*, Vol. 42, No. 10, pp. 6416-6423.
- Cohen, R. E. (1992). Origin of ferroelectricity in perovskite oxides. *Nature*, Vol. 358, No. 6382, pp. 136-138.
- Damjanovic, D. (2010). A morphotropic phase boundary system based on polarization rotation and polarization extension. *Appl. Phys. Lett.*, Vol. 97, No. 6, p. 062906 (3 pages).
- Diéguez, O., Rabe, K. M., & Vanderbilt, D. (2005). First-principles study of epitaxial strain in perovskites. *Phys. Rev. B*, Vol. 72, No. 14, p. 144101 (9 pages), and references therein.
- Fujii, Y., Uwe, H. & Sakudo, T. (1987). Stress-Induced Quantum Ferroelectricity in  $SrTiO_3$ . *J. Phys. Soc. Jpn.*, Vol. 56, No. 6, pp. 1940-1942.
- Furuta, T & Miura, K. (2010). First-principles study of ferroelectric and piezoelectric properties of tetragonal  $SrTiO_3$  and  $BaTiO_3$  with in-plane compressive structures. *Solid State Commun.*, Vol. 150, No. 47-48, pp. 2350-2353.
- Gonze, X., Beuken, J.-M., Caracas, R., Detraux, F., Fuchs, M., Rignanese, G.-M., Sindic, L., Verstraete, M., Zerah, G., Jollet, F., Torrent, M., Roy, A., Mikami, M., Ghosez, Ph., Raty, J.-Y. & Allan, D. C. (2002). First-principles computation of material properties: the ABINIT software project. *Comput. Mater. Sci.*, Vol. 25, No. 3, pp. 478-492.
- Gonze, X. et al. (2005). Informations on the Troullier-Martins pseudopotentials.  
**URL:** [http://www.abinit.org/downloads/psp-links/lda\\_tm\\_psp1\\_data](http://www.abinit.org/downloads/psp-links/lda_tm_psp1_data)
- Haeni, J. H., Irvin, P., Chang, W., Uecker, R., Reiche, P., Li, Y. L., Choudhury, S., Tian, W., Hawley, M. E., Craigo, B., Tagantsev, A. K., Pan, X. Q., Streiffer, K., Chen, L. Q., Kirchoefer, S. W., Levy, J. & Schlom, D. G. (2004). Room-temperature ferroelectricity in strained  $SrTiO_3$ . *Nature*, Vol. 430, No. 7001, pp. 758-761.
- Hamann, D. R., Wu, X., Rabe, K. M. & Vanderbilt, D. (2005). Metric tensor formulation of strain in density-functional perturbation theory. *Phys. Rev. B*, Vol. 71, No. 3, p. 035117 (13 pages).
- Khenata, R., Sahnoun, M., Baltache, H., Rérat, M., Rashek, A. H., Illes, N. & Bouhafs, B. (2005). First-principle calculations of structural, electronic and optical properties of  $BaTiO_3$  and  $BaZrO_3$  under hydrostatic pressure. *Solid State Commun.*, Vol. 136, No. 2, pp. 120-125.
- Kornev, I. G., Bellaiche, L., Bouvier, P., Janolin, P.-E., Dkhil, B. & Kreisel, J. (2005). Ferroelectricity of Perovskites under Pressure. *Phys. Rev. Lett.*, Vol. 95, No. 19, p. 196804 (4 pages).
- Kuroiwa, Y., Aoyagi, S., Sawada, A., Harada, J., Nishibori, E., Tanaka, M. & Sakata, M. (2001). Evidence for Pb–O Covalency in Tetragonal  $PbTiO_3$ . *Phys. Rev. Lett.*, Vol. 87, No. 21 p. 217601 (4 pages).
- Miura, K. & Tanaka, M. (1998). Electronic structures of  $PbTiO_3$ : I. Covalent interaction between Ti and O ions. *Jpn. J. Appl. Phys.*, Vol. 37, No. 12A, pp. 6451-6459.



- Miura, K. (2002). Electronic properties of ferroelectric  $\text{SrBi}_2\text{Ta}_2\text{O}_9$ ,  $\text{SrBi}_2\text{Nb}_2\text{O}_9$ , and  $\text{PbBi}_2\text{Nb}_2\text{O}_9$  with optimized structures. *Appl. Phys. Lett.*, Vol. 80, No. 16, pp. 2967-2969.
- Miura, K., Kubota, M., Azuma, M. & Funakubo, H. (2009). Electronic and structural properties of  $\text{BiZn}_{0.5}\text{Ti}_{0.5}\text{O}_3$  *Jpn. J. Appl. Phys.*, Vol. 48, No.9, p. 09KF05 (4 pages).
- Miura, K., Furuta, T. & Funakubo, H. (2010a). Electronic and structural properties of  $\text{BaTiO}_3$ : A proposal about the role of Ti 3s and 3p states for ferroelectricity. *Solid State Commun.*, Vol. 150, No 3-4, pp. 205-208.
- Miura, K., Kubota, M., Azuma, M. & Funakubo, H. (2010b). Electronic, structural, and piezoelectric properties of  $\text{BiFe}_{1-x}\text{Co}_x\text{O}_3$ . *Jpn. J. Appl. Phys.*, Vol. 49, No.9, p. 09ME07 (4 pages).
- Miura, K. & Furuta, T. (2010). First-principles study of structural trend of  $\text{BiMO}_3$  and  $\text{BaMO}_3$ : Relationship between tetragonal and rhombohedral structure and the tolerance factors. *Jpn. J. Appl. Phys.*, Vol. 49, No. 3, p. 031501 (6 pages), and references therein.
- Miura, K., Azuma, M. & Funakubo, H. (2011). [Review] Electronic and structural properties of  $\text{ABO}_3$ : Role of the B–O Coulomb repulsions for ferroelectricity. *Materials*, Vol. 4, No 1, pp. 260-273.
- Oguchi, T, Ishii, F. & Uratani, Y. (2009). New method for calculating physical properties from first principles–piezoelectric and multiferroics. *Butsuri*, Vol. 64, No. 4, pp. 270-276 (in Japanese).
- Perdew, J. P. & Wang, Y. (1992). Accurate and simple analytic representation of the electron-gas correlation energy *Phys. Rev. B*, Vol. 45, No. 23, pp. 13244-13249.
- Rappe, A. M. (2004). Opium–pseudopotential generation project.  
**URL:** <http://opium.sourceforge.net/index.html>
- Resta, R. (1994). Macroscopic polarization in crystalline dielectrics: the geometric phase approach. *Rev. Mod. Phys.*, Vol. 66, No. 3, pp. 899-915.
- Ricinschi, D., Kanashima, T. & Okuyama, M. (2006). First-principles study of tetragonality ratio and unit-cell volume influence on spontaneous polarization of  $\text{BaTiO}_3$  and  $\text{PbTiO}_3$ . *J. Soc. Mater. Sci. Jpn.*, Vol. 55, No. 2, pp. 169-172 (in Japanese).
- Shannon, R. D. (1976). Revised effective ionic radii and systematic studies of interatomic distances in halides and chalcogenides. *Acta Crystallogr., Sect. A*, Vol. 32, No. 5, pp. 751-767.
- Uratani, Y., Shishidou, T. & Oguchi T. (2008). First-principles calculations of colossal piezoelectric response in thin film  $\text{PbTiO}_3$ . *Ext. Abst. Jpn. Soc. Appl. Phys.*, Vol. 55, No. 2, p. 566 (in Japanese).
- Vanderbilt, D. (2000). Berry-phase theory of proper piezoelectric response. *J. Phys. Chem. Solids*, Vol. 61, No. 2, pp. 147-150, and references therein.
- Wu X., Vanderbilt, D. & Hamann, D. R. (2005). Systematic treatment of displacements, strains, and electric fields in density-functional perturbation theory. *Phys. Rev. B*, Vol. 72, No. 3, p. 035105 (13 pages).
- Wu, Z. & Cohen, R. E. (2005). Pressure-induced anomalous phase transitions and colossal enhancement of piezoelectricity in  $\text{PbTiO}_3$ . *Phys. Rev. Lett.*, Vol. 95, No. 3, p. 037601 (4 pages).



## **Ferroelectrics - Characterization and Modeling**

Edited by Dr. Mickaël Lallart

ISBN 978-953-307-455-9

Hard cover, 586 pages

**Publisher** InTech

**Published online** 23, August, 2011

**Published in print edition** August, 2011

Ferroelectric materials have been and still are widely used in many applications, that have moved from sonar towards breakthrough technologies such as memories or optical devices. This book is a part of a four volume collection (covering material aspects, physical effects, characterization and modeling, and applications) and focuses on the characterization of ferroelectric materials, including structural, electrical and multiphysic aspects, as well as innovative techniques for modeling and predicting the performance of these devices using phenomenological approaches and nonlinear methods. Hence, the aim of this book is to provide an up-to-date review of recent scientific findings and recent advances in the field of ferroelectric system characterization and modeling, allowing a deep understanding of ferroelectricity.

### **How to reference**

In order to correctly reference this scholarly work, feel free to copy and paste the following:

Kaoru Miura (2011). First-Principles Study of ABO<sub>3</sub>: Role of the B–O Coulomb Repulsions for Ferroelectricity and Piezoelectricity, *Ferroelectrics - Characterization and Modeling*, Dr. Mickaël Lallart (Ed.), ISBN: 978-953-307-455-9, InTech, Available from: <http://www.intechopen.com/books/ferroelectrics-characterization-and-modeling/first-principles-study-of-abo3-role-of-the-b-o-coulomb-repulsions-for-ferroelectricity-and-piezoelec>

**INTECH**  
open science | open minds

### **InTech Europe**

University Campus STeP Ri  
Slavka Krautzeka 83/A  
51000 Rijeka, Croatia  
Phone: +385 (51) 770 447  
Fax: +385 (51) 686 166  
[www.intechopen.com](http://www.intechopen.com)

### **InTech China**

Unit 405, Office Block, Hotel Equatorial Shanghai  
No.65, Yan An Road (West), Shanghai, 200040, China  
中国上海市延安西路65号上海国际贵都大饭店办公楼405单元  
Phone: +86-21-62489820  
Fax: +86-21-62489821

© 2011 The Author(s). Licensee IntechOpen. This chapter is distributed under the terms of the [Creative Commons Attribution-NonCommercial-ShareAlike-3.0 License](#), which permits use, distribution and reproduction for non-commercial purposes, provided the original is properly cited and derivative works building on this content are distributed under the same license.

IntechOpen

IntechOpen